J Solid State Electrochem (2012) 16:891–899
DOI 10.1007/s10008-011-1438-0

ORIGINAL PAPER

Effects of exposure time on the anodic dissolution of Monel-400 in aerated stagnant sodium chloride solutions

El-Sayed M. Sherif

Received: 15 March 2011 / Revised: 18 May 2011 / Accepted: 19 May 2011 / Published online: 7 June 2011

Abstract The anodic dissolution of Monel-400 (63.0% Ni, 28–34% Cu) alloy after its immersion in freely aerated stagnant 3.5% NaCl solutions for 0, 24, and 72 h has been investigated. The study was carried out using a variety of electrochemical techniques and gravimetric measurements after varied exposure periods (5–160 days). The work was complemented by scanning electron microscopy and energy dispersive X-ray analyzer (SEM/EDX) investigations. The electrochemical measurements showed that Monel suffers both general and pitting corrosion. The severity of uniform corrosion decreased, while pitting one increased with increasing the immersion time to 24 h and further to 72 h before measurements. Gravimetric data indicated that the weight loss increased, while the corrosion rate decreased for Monel with time. SEM images and EDX profile analyses confirmed that the corrosion of Monel after 160 days immersion in NaCl solutions occurs due to the selective dissolution of nickel.

Keywords Anodic dissolution · Electrochemical techniques · Gravimetric measurements · Monel-400 alloy · Microscopic investigations · Sodium chloride

E.-S. M. Sherif (✉)
Center of Excellence for Research in Engineering Materials (CEREM), College of Engineering, King Saud University, P. O. Box 800, Al-Riyadh 11421, Saudi Arabia
e-mail: esherif@ksu.edu.sa

E.-S. M. Sherif
Electrochemistry and Corrosion Laboratory, Department of Physical Chemistry, National Research Centre (NRC), Dokki, 12622 Cairo, Egypt

Introduction

Nickel–copper alloys are widely used as corrosion resistant materials in marine engineering. Their corrosion rates decrease sharply with increasing nickel content in the alloy. A series of Cu–Ni alloys have been studied in natural sea water and in chloride solutions under different conditions [1–9]. Some of these studies have [2] reported that selective electrodissolution of nickel is predominant; while others [7] have found that the dissolution of copper depends on the composition of the alloy under investigation.

Monel-400 is one of the most important nickel based alloys that contains about 60–70% nickel, 20–29% copper and small amounts of iron, manganese, silicon, and carbon. It is a solid solution alloy that can only be hardened by cold working. This alloy was discovered due to the efforts of Robert Crooks Stanley, who worked for the International Nickel Company in 1901. It was installed as a sheet roofing membrane in 1908. In the late 1920s, Monel-400 was begun to be used for grocery coolers, countertops, sinks, laundry and food preparation appliances, roofing and flashing.

Monel-400 is characterized by its good corrosion resistance, good weldability, and high strength. Therefore, it has been used extensively in many applications such as chemical processing equipment, gasoline and fresh water tanks, crude petroleum stills, valves and pumps, propeller shafts, marine fixtures and fasteners, electrical and electronic components, de-aerating heaters, process vessels and piping, boiler feed water heaters and other heat exchangers, and etc. [10–14]. For that when a piece of equipment needs to stand up to interior or exterior corrosive, Monel-400 is the fail-safe solution. It also has higher maximum working temperatures than nickel (up to 540 °C, and its melting point is 1,300–1,350 °C), which makes it the preferred

metal for boiler feed water heaters and other heat exchangers.

The objective of the present work was to study the effect of time of exposure on the anodic dissolution of Monel-400 in an open to air stagnant 3.5% sodium chloride solutions, which simulate natural sea water, using a variety of electrochemical and gravimetric measurements along with surface characterization. Although Monel-400 is known for its ability to stand up to tough corrosive elements, pitting corrosion of Monel-400 occurs when it is exposed to stagnant salt water such as seawater [15]. Which is why, a particular attention was paid to the effect of immersion time before measurements on the pitting corrosion of the alloy. Also, because pitting corrosion is one of the most destructive forms of localized corrosion besides the ability of chloride ions on the breakdown of any passive film might form on Monel-400.

Experimental procedure

Chemicals and electrochemical cell

A 3.5% sodium chloride solution was prepared from the as received 99.0% NaCl, Merck, to be used as the test electrolyte. An electrochemical cell with a three-electrode configuration was used for electrochemical measurements. A Monel-400 rod (was purchased from Magellan Metals, USA, with the following chemical composition, Ni–63.0% min, Cu–"28-34%" max, Fe–2.5% max, Mn–2.0%, Si–0.5% max, C–0.3% max, and S–0.024%) was used as a working electrode. A platinum foil and a Metrohm Ag/AgCl electrode (in 3 M KCl) were used as counter and reference electrodes, respectively.

Monel-400 rods for electrochemical measurements were prepared by welding a copper wire to a drilled hole was made on one face of the rod; the rod with the attached wire were then cold mounted in resin and left to dry in air for 24 h at room temperature. Before measurements, the other face of the Monel electrode that was not drilled was first grinded successively with metallographic emery paper of increasing fineness of up to 800 grits, and then polished with 1, 0.5, and 0.3 μm alumina slurries (Buehler). The electrodes were then washed with doubly distilled water, degreased with acetone, washed using doubly distilled water again and finally dried with tissue paper. In order to prevent the possibility of crevice corrosion during measurement, the interface between sample and resin was coated with Bostik Quickset, a polyacrelate resin. The diameter of the working electrode was 1.2 cm with a total exposed area of 1.13 cm^2.

Electrochemical methods

Electrochemical experiments were performed by using an Autolab Potentiostat (PGSTAT20 computer controlled) operated by the general purpose electrochemical software version 4.9. Cyclic potentiodynamic polarization (CPP) curves were obtained by scanning the potential in the forward direction from −800 to +800 mV vs. Ag/AgCl then backward from +800 to −800 mV again at the same scan rate, 3.0 mV/s. CA current–time experiments were carried out by stepping the potential at +100 mV versus Ag/AgCl for 120 min. For the PPC and CA tests, the curves were recorded after the electrode immersion in the test solution for 0, 24, and 72 h before measurements. Electrochemical impedance spectroscopy (EIS) tests were performed after 1, 24, and 72 h of the electrode immersion at an open-circuit potential over a frequency range of 100 kHz–10 mHz, with an AC wave of ±5 mV peak-to-peak overlaid on a DC bias potential, and the impedance data were collected using Powersine software at a rate of 10 points per decade change in frequency. All measurements were carried out at room temperature in freely aerated solutions.

Weight loss data

The weight loss experiments were carried out using rectangular Monel-400 coupons (was purchased in the form of sheets from Magellan Metals, USA, with the same chemical composition of Monel-400 rods) having a dimension of 4.0 cm length, 2.0 cm width, and 0.4 cm thickness and the exposed total area of 54.02 cm^2. The coupons were polished and dried as for the case of Monel-400 rods, weighed, and then suspended in 300 cm^3 solutions of 3.5% NaCl for different exposure periods (5–160 days). The losses in weight per area (ΔW, g cm^{-2}) and the corrosion rates (K_{Corr}, millimeters/year (mmpy)) over the exposure time were calculated as follows [16]:

$$\Delta W = \frac{W_1 - W_2}{A} \tag{1}$$

$$K_{Corr} = \frac{\Delta W K}{D t} \tag{2}$$

Where, W_1 and W_2 are the weighs of the Monel-400 coupon per gram before and after its immersion in the test solution, A is the area of the Monel-400 coupon per square centimeter, K is a constant that defines the unit of the corrosion rate (K=87,600 for the mmpy unit), D is the density of Monel-400 per gram per cubic centimeter, and t is the immersion time per hour.

Scanning electron microscopy investigation and energy dispersive X-ray analyzer analysis

The scanning electron microscopy (SEM) investigation and energy dispersive X-ray (EDX) analysis were obtained on the surface of a Monel-400 coupon after its immersion in open to air stagnant 3.5% NaCl solution for 160 days. The SEM images were carried out by using a JEOL model JSM-6610LV (Japanese made) scanning electron microscope with an energy dispersive X-ray analyzer attached.

Results and discussion

Open-circuit potential measurements

The variation of the open-circuit potential (OCP) versus time (72 h) for Monel-400 electrode in aerated stagnant 3.5% NaCl solution is presented in Fig. 1. The OCP of Monel showed a rapid shift towards the negative direction in the first 25 h. This negative shift perhaps reflects the dissolution of Monel-400 under the corrosive nature of the chloride ions. Increasing the time further led to a very slight shift in the OCP values and up to the end of the run, which might be due to the formation of corrosion products on the alloy surface. The formation of such corrosion products partially protected the alloy surface and decreased its uniform corrosion with time.

CPP measurements

In order to obtain the corrosion parameters like corrosion potential (E_{Corr}), corrosion current (j_{Corr}), pitting potential (E_{Pit}), pitting current (j_{Pit}), polarization resistance (R_P), and K_{Corr} of Monel-400 in 3.5% NaCl solutions after different exposure intervals, CPP experiments were carried out. The CPP curves for Monel-400 after (a) 0 h, (b) 24 h, and (c) 72 h immersion in 3.5% NaCl solutions are shown in Fig. 2. It is well-known that the cathodic reaction for

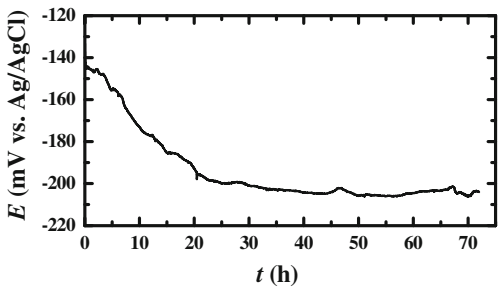

Fig. 1 Changes of the open-circuit potential versus time (72 h) for Monel-400 in an open to air stagnant 3.5% NaCl solution

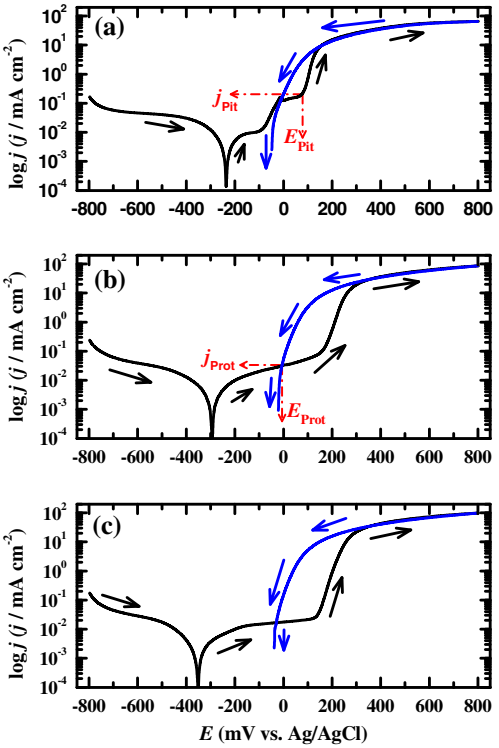

Fig. 2 Cyclic potentiodynamic polarization curves for Monel-400 after its immersion in aerated stagnant 3.5% NaCl solutions for 0 h (**a**), 24 h (**b**), and 72 h (**c**), respectively

Monel-400 in aerated near neutral solutions is the oxygen reduction as follows:

$$2H_2O + O_2 + 4e^- \rightleftarrows 4OH^- \quad (3)$$

Whereas, and according to Blundy and Pryor [5] and Francis et al. [17], the anodic reaction of Monel-400 is the selective dissolution of nickel, particularly at high potential values. It is clearly seen from Fig. 2a that an active dissolution of the alloy occurred with increasing potential in the anodic side. It is also seen that there is a peak on the anodic branch at which the current decreased with increasing the applied potential. This peak was appeared due to either the formation of a passive oxide film [18, 19] or the accumulation of corrosion products on the electrode surface. The sudden increase of the current after the formation of the peak is due to the breakdown of the passive film formed on the Monel-400 surface by the chloride ions attack, which led to the occurrence of pitting corrosion [20, 21]. The further increase of the current with potential is caused by the agglomeration of chloride ions inside the pits leading to pit growth and ultimately substrate alloy dissolution [15].

Increasing the exposure time of the electrode to 24 h before measurements decreased both the cathodic and

anodic currents and eliminated the peak that was appeared on curve a. This effect increased significantly when the immersion time was increased to 72 h as shown in Fig. 2c. The corrosion parameters obtained from Fig. 2 are listed in Table 1. The values of E_{Corr} and j_{Corr} were obtained from the extrapolation of anodic and cathodic Tafel lines located next to the linearized current regions. E_{Pit} was determined from the forward anodic polarization curves where a stable increase in the current density occurs and the j_{Pit} value is the corresponding current to E_{Pit}. The protection potential (E_{Prot}) and protection current (j_{Prot}) were determined from the backward anodic polarization curve at the intersection point with the forward polarization curve. Furthermore, the way by which E_{Pit}, j_{Pit}, E_{Prot}, and j_{Prot} is shown on Fig. 2. It is seen from Table 1 that the values of j_{Corr}, j_{Prot}, and j_{Pit} decreased with increasing the immersion time. Also, the values of E_{Corr}, E_{Prot}, and E_{pit} increased to the more negative values. This effect also increased the values of R_P and decreased the values of K_{Corr}; R_P and K_{Corr} were calculated from the polarization data as follows [16, 22–24]:

$$R_P = \frac{1}{j_{Corr}}\left(\frac{\beta_c.\beta_a}{2.3(\beta_c+\beta_a)}\right) \quad (4)$$

$$K_{Corr} = \frac{j_{Corr}\, k\, E_W}{d\, A} \quad (5)$$

Where, j_{Corr} is the corrosion current density, β_c and β_a are the cathodic and anodic Tafel slopes, respectively, k is a constant that defines the units for the corrosion rate (=3,272 mm/(amp cm year)), E_W the equivalent weight in grams/equivalent of Monel-400 alloy (calculated E_W=30.8 grams/equivalent), d the density in g cm^{-3} (=8.83), and A the area of the exposed surface of the electrode in square centimeter.

The positive shift in the E_{Corr} is apparently due to decreasing the rate of the anodic reactions as a result of the accumulation of corrosion products and oxide film on the Monel surface, which agrees with the OCP measurements at the same exposure time. The increases in the β_c and β_a are related to the decrease in both the cathodic and anodic currents as a result of the decrease in their corrosion reactions, respectively. As well as, the decreases in cathodic, j_{Corr} and anodic currents and K_{Corr} with increasing the immersion time are mainly due to the decrease of the chloride ion attack on the surface, which led to the decrease of the uniform corrosion of Monel. Furthermore, the increase of the area of the hysteresis loop with increasing time is due to the increase of pitting corrosion of the alloy.

Chronoamperometric measurements

In order to study the pitting corrosion of Monel-400 after varied exposure periods in the stagnant chloride solutions at a more positive potential value, chronoamperometric current–time experiments were carried out at 100 mV. The variation of the measured dissolution currents versus time for Monel-400 electrode that was immersed in the aerated 3.5% NaCl solutions for 0 h (1), 24 h (2), and 72 h (3), respectively, before stepping the potential to 100 mV for 120 min are shown in Fig. 3. The value of the constant potential was determined from polarization curves. The highest current values for Monel were recorded when the measurements were carried out after the first moment of the electrode immersion, curve 1. In this case, the current showed a rapid increase in its initial values in the first 4 min due to the dissolution of a peroxide film that might have formed on the surface in air before electrode immersion. The current then slightly decreased before increasing slowly again to the end of the run. The decrease of current is due to the formation of corrosion products on the alloy surface ceases the Monel dissolution, while the gradual increase of current is due to the initiation then propagation of pitting corrosion.

Increasing the immersion time to 24 h, curve 2, led to decreasing the absolute current and further current decreases were recorded when the time was increased to 72 h. This decrease of current with immersion time can be explained by the formation of a passive oxide film and/or corrosion products; this film gets thicker as the time increases before applying the constant potential. The formation of such a film also decreases the uniform attack on the Monel-400 surface and so decreases the absolute current under the applied potential. In general, the increase

Table 1 Corrosion parameters obtained from CPP curves shown in Fig. 2 for the Monel-400 alloy in aerated stagnant 3.5% NaCl solutions after different exposure intervals

Parameter medium	E_{Corr}/ mV	j_{Corr}/ μAcm^{-2}	β_c/ mVdec^{-1}	β_a / mVdec^{-1}	E_{Prot}/ mV	j_{Prot}/ μAcm^{-2}	E_{Pit}/ mV	j_{Pit}/ μAcm^{-2}	R_p/ Ωcm^2	K_{Corr}/ mmy^{-1}
NaCl (0 h)	−230	6.5	120	110	−2	155	80	200	3,839	0.074
NaCl (24 h)	−290	3.6	115	125	−10	35	150	75	7,234	0.041
NaCl (72 h)	−350	2.2	105	115	−31	15	140	20	10,847	0.025

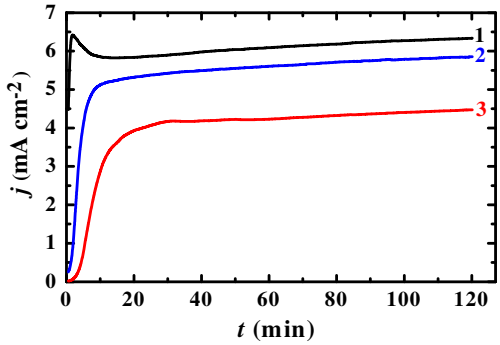

Fig. 3 Chronoamperometric curves for Monel-400 electrode that has been immersed in aerated stagnant 3.5% NaCl solutions for 0 h (*1*), 24 h (*2*), and 72 h (*3*), respectively, before applying a potential value of 100 mV vs. Ag/AgCl for 120 min

of current values with time for the Monel-400 at all exposure intervals is due to the occurrence of the pitting corrosion. Pits develop at sites where oxygen adsorbed on the alloy surface is displaced by an aggressive species such as Cl^- ions that are presented in the solution [15, 25]. This is because Cl^- ions have small diameters allows it to penetrate through the protective oxide film and displace oxygen at the sites where metal–oxygen bond is the weakest [15, 26, 27].

EIS measurements

The EIS measurements were carried out to determine kinetic parameters for electron transfer reactions at the Monel-400/electrolyte interface and to confirm the data obtained by polarization and chronoamperometric measurements. We have successfully employed the method to explain the corrosion and corrosion inhibition of several metals and alloys in chloride media [16, 22–24, 28–37]. The Nyquist plots (a), Bode (b), and phase angle (c), respectively, for Monel-400 after its immersion for 1 h (1), 24 h (2), and 72 h (3) in aerated stagnant 3.5% NaCl solutions are shown in Fig. 4. The impedance spectra of the Nyquist plots shown in Fig. 4a were analyzed by fitting to the equivalent circuit model shown in Fig. 5. This circuit was also used to fit the impedance data obtained for Monel-400 in simulated seawater as reported by Klassen et al. [38]. The parameters obtained by fitting the equivalent circuit shown in Fig. 5 are listed in Table 2. Here, R_S represents the solution resistance between the Monel-400 and the counter (platinum) electrode, Q the constant phase elements (CPEs) and contain two parameters; a pseudo capacitance and an exponent (an exponent of less than unity indicates a dispersion of capacitor effects [38]), the R_{P1} accounts for the resistance of a film layer formed on the Monel-400 surface, C_{dl} is the double-layer capacitance, and R_{P2} accounts for the charge transfer resistance at the alloy surface, i.e., the polarization resistance.

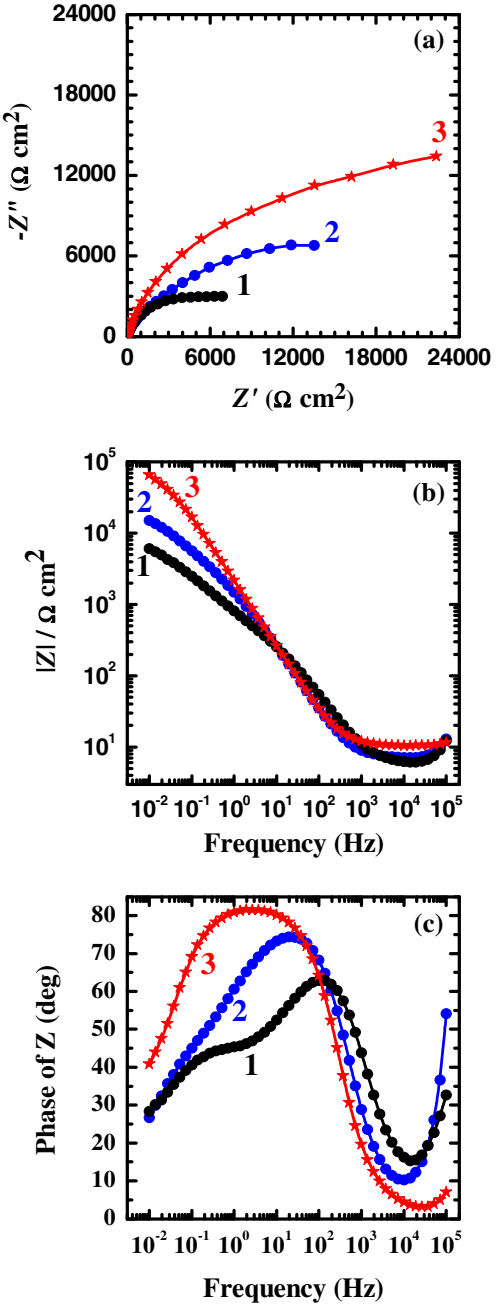

Fig. 4 Nyquist (**a**), Bode (**b**), and phase angle (**c**) plots for Monel-400 at OCP after its immersion in aerated stagnant 3.5% NaCl solutions for 1 h (*1*), 24 h (*2*), and 72 h (*3*), respectively

It is subtly evident from Fig. 4a that the Nyquist plots recorded only one semicircle for Monel-400 in all chloride solutions. Increasing the exposure time before measurement led to increasing the diameter of the semicircle meaning that the resistance of Monel against general corrosion increases with increasing time. The semicircles at high frequencies in Fig. 4a are generally associated with the relaxation of electrical double-layer capacitors and the diameters of the high-frequency semicircles can be consid-

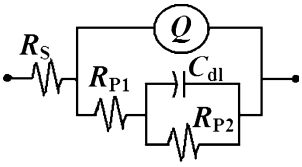

Fig. 5 The equivalent circuit used to fit the experimental data presented in Fig. 4a. See text for symbols used in the circuit

ered as the charge transfer resistance [23, 39]. It is also seen from the values of elements of the equivalent circuit model, Fig. 5, which are listed in Table 2 that R_S, R_{P1}, and R_{P2} increased with increasing the immersion time. This increase in Monel resistances is attributed to the formation of a passive film and/or corrosion products, which gets thicker with time and could lead to the decrease in j_{Corr} and K_{Corr}, and also the increase in R_P values we have seen in polarization data (Fig. 2 and Table 1) under the same conditions. The polarization resistance measured by EIS is a measure of the uniform corrosion rate as opposed to tendency towards localized corrosion. The decrease of CPEs and C_{dl} values with time confirms also the decrease of Monel uniform corrosion. The high C_{dl} value measured for Monel after 1 h immersion in the chloride solution compared to its value in case of 24 and 72 h, was probably due to its having the highest percentage of experimental error obtained from fitting the EIS Nyquist data to the equivalent circuit model (Fig. 5). It is also observed that increasing the immersion time results in an increase in the impedance of the interface ($-Z$|, Fig. 4b) and the maximum phase angle (Fig. 4c). It has been reported that the reason for the increase in the values of $|Z|$, especially at the low-frequency regions, is the increased surface passivation, which in this case resulted from prolonging the exposure period [40–42].

Weight loss data and SEM/EDX investigations

The variations of (a) weight loss (ΔW, g cm^{-2}) and (b) K_{Corr} (mmpy), respectively vs. time for Monel-400 coupons in 300 cm^3 of aerated stagnant 3.5% NaCl solutions are shown in Fig. 6. The values of ΔW and K_{Corr} were calculated using Eqs. 1 and 2, respectively. One can see that the values of ΔW increased with time due to the aggressiveness attack of the chloride ions toward the Monel surface. Opposite to that,

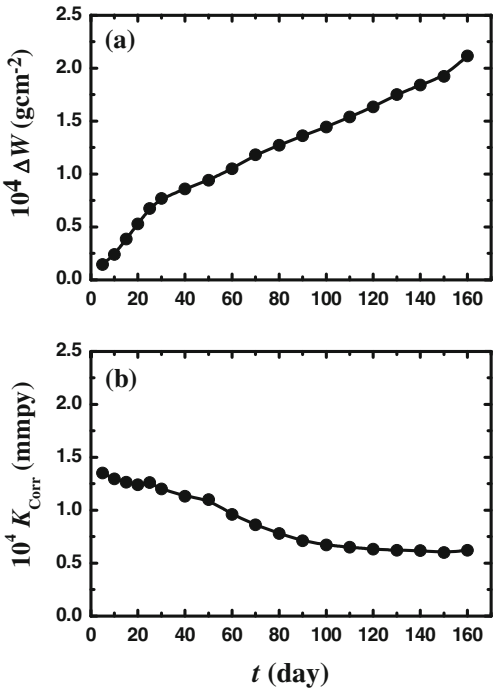

Fig. 6 Variation of the weight loss (**a**) and corrosion rate (**b**) versus time for Monel-400 coupons in freely aerated stagnant 3.5% NaCl solutions

the K_{Corr} values decreased, which proves the decrease of the uniform corrosion and agrees with the polarization, chronoamperometry, and EIS data we have seen earlier.

In order to see the surface morphology and to identify the composition of the species formed on the Monel-400 surface after its immersion in aerated stagnant 3.5% NaCl, SEM/EDX investigations were carried out. Figure 7 depicts the SEM micrographs for Monel surface after its immersion for 160 days in the test solution, (a) a large area of the surface, (b) an extended dark area, and (c) an extended white area. The corresponding EDX profile analyses are shown in Figs. 8a–c, respectively. It is clearly seen from the SEM images presented in Fig. 7 that there are black and white areas with no pits observed on the Monel surface. The atomic percentage of the elements found in the area shown in Fig. 7a and displayed in the EDX profile presented in Fig. 8a, were 54.02% O, 27.29% Cl, 14.30%

Table 2 EIS parameters obtained by fitting the Nyquist plots shown in Fig. 4a with the equivalent circuit shown in Fig. 5 for the Monel-400 in aerated stagnant 3.5% NaCl solutions after different exposure intervals

Parameter medium	R_S/Ωcm^2	Q (CPEs)		R_{P1}/Ωcm^2	C_{dl}/μFcm^{-2}	R_{P2}/Ωcm^2
		Y_Q/μFcm^{-2}	n			
NaCl (1 h)	4.89	22.07	0.70	3,344	3.146	8,583
NaCl (24 h)	7.32	17.14	0.75	7,559	0.413	12,103
NaCl (72 h)	9.74	13.10	0.80	11,543	0.085	21,300

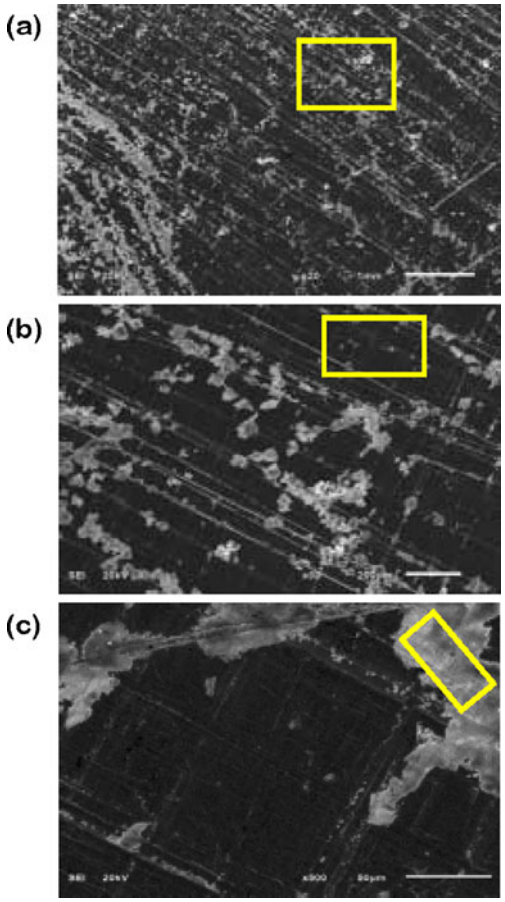

Fig. 7 SEM micrographs for Monel-400 surface after its immersion in 3.5% NaCl solutions for 160 days; (**a**) SEM image for a large area of the surface, (**b**) SEM image for an extended *dark area*, and (**c**) SEM image for an extended *white area*, respectively

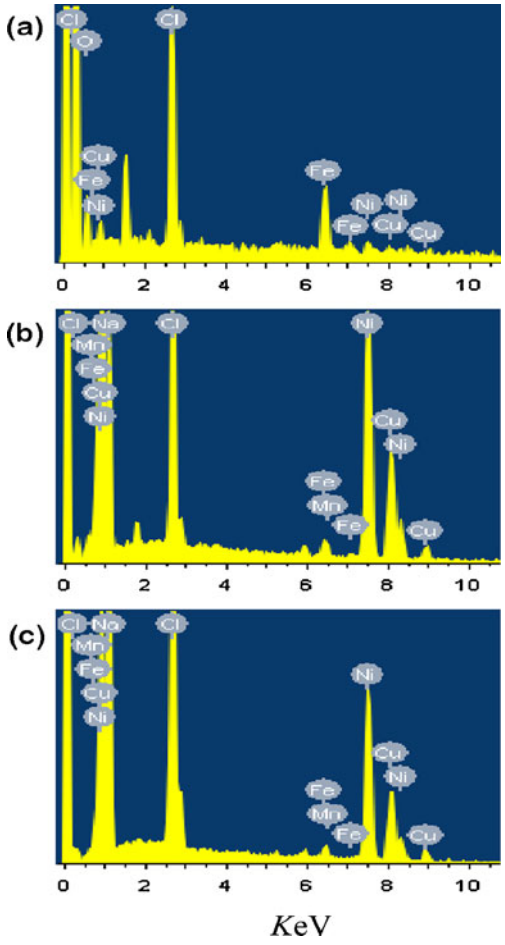

Fig. 8 The corresponding EDX profile analyses for the Monel surface in the selected areas shown in Fig. 7a–c, respectively

Fe, 2.90% Ni, and 1.48% Cu. The very low content of the main Monel components (Ni and Cu) and high content of Fe mean that the surface is fully covered with thick iron oxide film and chloride and/or oxy-chloride compounds and complexes. Also, the corrosion of Monel went via the selective electrodissolution of Ni as has been reported by Lee and Nobe [2].

On the other hand, the atomic percentages of the elements found in the investigated dark area of SEM image shown in Fig. 7b and displayed in the EDX profile depicted in Fig. 8b, were 65.63% Ni, 31.03% Cu, 2.29% Fe, and 1.15% Mn. This indicates that the surface in this area is containing the main alloying elements having almost their actual percentages. The atomic percentage of the elements found in the investigated white area as seen in Fig. 7c and represented by the EDX profile shown in Fig. 8c were 56.24% Na, 21.18% Cl, 14.25% Ni, 6.86% Cu, 0.59% Fe, and 0.27% Mn and indicated that only sodium chloride salt is presented in this area.

Conclusions

The effect of different exposure intervals on the anodic dissolution of Monel-400 alloy in freely aerated stagnant 3.5% NaCl solutions has been reported. Polarization and chronoamperometric measurements revealed that uniform corrosion decreases, while the pitting corrosion increases with increasing the immersion time. Impedance spectra revealed that increasing the exposure time increases the surface and polarization resistances. The increase of the weight loss and the decrease of the corrosion rate of Monel gave further confirmation for the data obtained by the electrochemical measurements. SEM/EDX investigations after 160 days proved that the surface of Monel develops a mixture of most probably oxides, chlorides, and/or oxy-chloride complexes with a selective dissolution of Ni. Results, together, are in good agreement confirmed clearly that the increase of exposure time of Monel in aerated 3.5% NaCl solutions decreases uniform corrosion and increasing the pitting one.

Acknowledgments This project was supported by King Saud University, Deanship of Scientific Research, College of Engineering Research Center.

References

1. Ali JA (1994) Rotating ring-ring electrode study of copper component dissolution behaviour in air-saturated 0.5 M NaCl solution. Corros Sci 36:773–783
2. Lee HP, Nobe K (1984) Rotating ring-disk electrode studies of Cu-Ni alloy electrodissolution in acidic chloride solutions. J Electrochem Soc 131:1236–1243
3. North RF, Pryor MJ (1970) The influence of corrosion product structure on the corrosion rate of Cu–Ni alloys. Corros Sci 10:297–311
4. Walton ME, Brook PA (1977) The dissolution of Cu–Ni alloys in hydrochloric acid—I. Rotating disc electrode measurements. Corros Sci 17:317–328
5. Blundy RG, Proyor MJ (1972) The potential dependence of reaction product composition on copper–nickel alloys. Corros Sci 12:65–75
6. Kato C, Atteya BG, Castle JE, Pickering HW (1980) On the mechanism of corrosion of Cu-9.4Ni-1.7Fe alloy in air saturated aqueous NaCl solution. J Electrochem Soc 127:1890–1896
7. Petetin S, Crousier J, Crousier JP (1984) Comportement de l'alliage Cuivre-nickel 70/30 dans une solution de NaCl A 3%. Mater Chem Phys 10:317–329
8. Li W, Nobe K (1993) Electrodissolution kinetics of iron in chloride solutions. J Electrochem Soc 140:1642–1650
9. Milošev I, Metikoš-Huković M (1992) Factors influencing the breakdown susceptibility of the passive film on Cu–Ni alloy. Corrosion 48:185–193
10. Ulig HH (1963) Corrosion and corrosion control. Wiley, New York
11. Ghosh SK, Dey GK, Dusane RO, Grover AK (2006) Improved pitting corrosion behaviour of electrodeposited nanocrystalline Ni–Cu alloys in 3.0 wt.% NaCl solution. J Alloy Compd 426:235–243
12. Rangarajan S, Bera S, Narasimhan SV (1998) Electrochemical and surface analytical study of the formation of oxide films on monel-400 and copper in alkaline media. J Solid State Electrochem 2:94–98
13. Gagg CR, Lewis PR (2008) Environmentally assisted product failure—synopsis and case study compendium. Eng Fail Anal 15:505–520
14. Malik AU, Ahmad S, Andijani I, Al-Fouzan S (1999) Corrosion behavior of steels in Gulf seawater environment. Desalination 123:205–213
15. Gouda VK, Selim IZ, Khedr AA, Fathi AM (1999) Pitting corrosion behaviour of Monel-400 alloy in chloride solutions. Mater Sci Technol 15:208–212
16. Sherif EM, Park SM (2006) 2-Amino-5-ethyl-1,3,4-thiadiazole as a corrosion inhibitor for copper in 3.0% NaCl solutions. Corros Sci 48:4065–4079
17. Francis JT, McIntyre NS, Davidson RD, Ramamurthy S, Brennenstühl AM, McBride A, Roberts A (2002) Mechanisms for pitting corrosion in alloy N04400 as revealed by imaging XPS, ToF-SIMS and low-voltage SEM. Surf Interface Anal 33:29–34
18. Friend WZ (ed) (1980) Corrosion of nickel and nickel-based alloys. NACE International, Houston, TX
19. Stern M (1959) Evidence for a logarithmic oxidation process for stainless steel in aqueous systems. J Electrochem Soc 106:376–381
20. Streicher MA (1956) Pitting corrosion of 18Cr-8Ni stainless steel. J Electrochem Soc 103:375–390
21. Schwenk W (1964) Theory of stainless steel pitting. Corrosion 20:129t–137t
22. Sherif EM, Park SM (2005) Inhibition of copper corrosion in 3.0% NaCl solution by *N*-phenyl-1,4-phenylenediamine. J Electrochem Soc 152:B428–B433
23. Sherif EM, Park SM (2006) Effects of 2-amino-5-ethylthio-1,3,4-thiadiazole on copper corrosion as a corrosion inhibitor in aerated acidic pickling solutions. Electrochim Acta 51:6556–6562
24. Sherif EM, Park SM (2006) Inhibition of copper corrosion in acidic pickling solutions by *N*-phenyl-1,4-phenylenediamine. Electrochim Acta 51:4665–4673
25. Bohni H, Uhlig HH (1969) Environmental factors affecting the critical pitting potential of aluminum. J Electrochem Soc 116:906–910
26. Ali JA, Ambrose JR (1992) The relationship between copper component dissolution kinetics and the corrosion behaviour of monel-400 alloy in de-aerated NaCl solutions. Corros Sci 33:1147–1159
27. Rozenfeld IL, Marshakov IK (1964) Mechanism of crevice corrosion. Corrosion 20:115t–125t
28. Sherif EM (2006) Effects of 2-amino-5-(ethylthio)-1,3,4-thiadiazole on copper corrosion as a corrosion inhibitor in 3% NaCl solutions. Appl Surf Sci 252:8615–8623
29. Sherif EM, Almajid AA (2010) Surface protection of copper in aerated 3.5% sodium chloride solutions by 3-amino-5-mercapto-1,2,4-triazole as a copper corrosion inhibitor. J Appl Electrochem 40:1555–1562
30. Sherif EM (2010) Corrosion mitigation of copper in acidic chloride pickling solutions by 2-amino-5-ethyl-1,3,4-thiadiazole. J Mater Eng Perform 19:873–879
31. Sherif EM, Erasmus RM, Comins JD (2010) In situ Raman spectroscopy and electrochemical techniques for studying corrosion and corrosion inhibition of iron in sodium chloride solutions. Electrochim Acta 55:3657–3663
32. Sherif EM, Almajid AA, Latif FH, Junaedi H (2011) Effects of graphite on the corrosion behavior of aluminum–graphite composite in sodium chloride solutions. Inter J Electrochem Sci 6:1085–1099
33. Sherif EM, Ahmed AH (2010) Synthesizing new hydrazone derivatives and studying their effects on the inhibition of copper corrosion in sodium chloride solutions. Synth React Inorg Met-Org Nano-Metal Chem 40:365–372
34. Sherif EM (2011) Corrosion and corrosion inhibition of aluminum in Arabian Gulf seawater and sodium chloride solutions by 3-amino-5-mercapto-1,2,4-triazole. Inter J Electrochem Sci 6:1479–1492
35. Sherif EM, Erasmus RM, Comins JD (2008) Inhibition of copper corrosion in acidic chloride pickling solutions by 5-(3-aminophenyl)-tetrazole as a corrosion inhibitor. Corros Sci 50:3439–3445
36. Sherif EM, Potgieter JH, Comins JD, Cornish L, Olubambi PA, Machio CN (2009) Effects of minor additions of ruthenium on the passivation of duplex stainless-steel corrosion in concentrated hydrochloric acid solutions. J Appl Electrochem 39:83–91
37. Sherif EM, Potgieter JH, Comins JD, Cornish L, Olubambi PA, Machio CN (2009) The beneficial effect of ruthenium additions on the passivation of duplex stainless steel corrosion in sodium chloride solutions. Corros Sci 51:1364–1371
38. Klassen RD, Roberge PR, Wang Y (2005) Corrosion Resistance of UNS NO4400 vs. electroless nickel in simulated marine service. Corrosion (NACE) Paper No. 05232

39. Ma H, Chen S, Niu L, Zhao S, Li S, Li D (2002) Inhibition of copper corrosion by several Schiff bases in aerated halide solutions. J Appl Electrochem 32:65–72
40. Sherif EM, Erasmus RM, Comins JD (2007) Effects of 3-amino-1,2,4-triazole on the inhibition of copper corrosion in acidic chloride solutions. J Colloid Interface Sci 311:144–151
41. Sherif EM, Erasmus RM, Comins JD (2007) Corrosion of copper in aerated acidic pickling solutions and its inhibition by 3-amino-1,2,4-triazole-5-thiol. J Colloid Interface Sci 306:96–104
42. Sherif EM, Erasmus RM, Comins JD (2007) Corrosion of copper in aerated synthetic sea water solutions and its inhibition by 3-amino-1,2,4-triazole. J Colloid Interface Sci 309:470–477